Potential of femtosecond chirp control of ultrabroadband semiconductor continuum nonlinearities

J. Kunde, U. Siegner, S. Arlt, G. Steinmeyer, F. Morier-Genoud, and U. Keller

Swiss Federal Institute of Technology Zurich, Institute of Quantum Electronics, ETH Hönggerberg HPT, CH-8093 Zurich, Switzerland

Received February 23, 1999; revised manuscript received May 19, 1999

We present an experimental study of the influence of frequency chirp in 20-fs optical pulses on broadband semiconductor continuum nonlinearities. Differential-transmission (DT) measurements were performed in which either the exciting pump pulse or the readout probe pulse, or both pump and probe, were chirped. We demonstrate that in certain chirp configurations the spectrally integrated DT is enhanced on an ultrafast time scale compared with measurements with unchirped pulses. Therefore pulse chirping has the potential to improve and optimize all-optical ultrafast switching. Spectrally resolved DT measurements explain these findings. Positive and negative DT contributions are observed in different spectral ranges. The spectral position and the magnitude of these contributions change in time. Proper chirping of the pulses optimizes the readout of the positive contributions and maximizes the spectrally integrated DT. A simple quantitative model confirms these considerations. © 1999 Optical Society of America [S0740-3224(99)00312-4]

OCIS codes: 320.1590, 320.7110, 320.7130.

1. INTRODUCTION

Ultrafast light–semiconductor interaction has been studied intensively in recent years.[1] This research was driven by the interest in fundamental physical questions and by the need to characterize light–semiconductor interaction for device applications. One important technology related to ultrafast semiconductor optics is all-optical switching.[2,3] In ultrafast all-optical switching devices the optical nonlinearity of a semiconductor is exploited. Various possibilities exist for the manipulation of this nonlinearity, in which the common approach is to change the material itself or the device structure. For example, low-temperature growth results in fast carrier trapping and short recovery times of the optical nonlinearity in GaAs.[4] With respect to the device structure, for example, electronic confinement enhances the excitonic nonlinearity in quantum wells.[5] In this paper we demonstrate an alternative, complementary possibility for manipulating the ultrafast optical nonlinearity of semiconductors. In our approach a frequency chirp is imposed on femtosecond ultrabroadband laser pulses and is used to manipulate the optical nonlinearity. In a frequency-chirped pulse the different frequency components, which make up the broadband pulse, are distributed over the temporal pulse profile. It is shown that frequency chirp is an additional experimental control parameter for light–semiconductor interaction. This concept is referred to as coherent control.[6]

For future ultrafast semiconductor devices operating on the 10-fs time scale, broadband-continuum nonlinearities are important, rather than narrow-band excitonic nonlinearities. Therefore our work is focused on the broadband-continuum nonlinearity. We investigate the interaction between chirped ultrafast optical pulses and semiconductor-continuum transitions in differential-transmission (DT) measurements. Semiconductor DT spectroscopy with chirped pulses has been reported previously.[7,8] However, in Ref. 7 only the influence of a probe-pulse frequency chirp on the coherent excitonic nonlinearity is investigated. In Ref. 8, only DT spectra taken with chirped pump pulses were examined to discriminate between coherent and carrier effects in semiconductors. We like to stress that, for most device applications, the enhancement of the spectrally integrated (SI) DT is most important. In Ref. 9 we have already shown that an enhancement of the SI DT signal can be achieved in an ultrafast (20–50-fs) switching window with equally chirped pump and probe pulses. In this paper we explore the full potential of chirp control of the SI DT in all possible chirp configurations for ultrabroadband-continuum excitation and pinpoint the most relevant physical mechanisms for chirp control. We will determine the appropriate chirp configuration to enhance the SI DT signal.

Our results show that all-optical switching schemes can benefit from the controlled usage of pulse chirping. For example, in a single-pulse setup, chirping can be advantageous for femtosecond laser-pulse generation when the broadband nonlinear optical response of semiconductors is used as a saturable absorption mechanism.[10] Here, a proper chirp can optimize the absorber modulation in ultrafast switching windows. This facilitates pulse formation. Moreover, in all-optical fiber communication systems, one often has to deal with chirped pulses. The knowledge of chirp effects is then important to evaluate signal-processing schemes in the presence of pulse chirp. Furthermore, chirp effects are important for fundamental studies in which a residual chirp can mask the true dynamics. Because the complete elimination of

chirp becomes more and more difficult for today's sub-10-fs pulses, the knowledge of chirp effects becomes increasingly important.

The paper is organized as follows. In Section 2 we discuss the experimental technique and the methods used for pulse chirping and pulse characterization. The experimental results are presented in Section 3. In Subsection 3.A we present the results of SI DT measurements when either the pump pulse or the probe pulse, or both pump and probe, are chirped. The results are compared with SI DT measurements by use of unchirped pulses. To explain the SI DT data, we performed extensive spectrally resolved DT (SR DT) measurements. We first recall the properties of the SR DT for unchirped pulses (Subsection 3.B) and then show how the dynamics is influenced by the chirp. Subsection 3.C discusses experiments in which both the pump and the probe pulses are chirped, while Subsection 3.D describes experiments in which only one pulse is chirped. Throughout Section 3, the chirp effects are explained by qualitative arguments. This is done to provide a first insight into the most important effects responsible for the observed chirp influence. In Section 4 a simple quantitative model is presented that confirms the qualitative arguments. We finally present our conclusions in Section 5.

2. EXPERIMENT

We measured the pump-induced transmission change $\Delta T = T_{\text{Pump on}} - T_{\text{Pump off}}$ in noncollinear pump–probe measurements. The pump and the probe pulses from a Ti:sapphire laser have identical spectra centered at 1.57 eV with a spectral FWHM of 110 meV and a bandwidth-limited pulse duration of 20 fs. The pump and the probe are linearly cross polarized.

We can carefully control the total group-delay dispersion (GDD) of our setup with double-chirped mirrors,[11] a pair of fused-silica prisms, and fused-silica substrates. Depending on the total GDD, unchirped or chirped pulses can be obtained. Interferometric and noncollinear background-free autocorrelation measurements allow us to determine whether bandwidth-limited pulses have been obtained at the position of the sample. The pulse duration of bandwidth-limited pulses is calculated as the Fourier transform of the pulse spectrum under the assumption of a constant spectral phase. Likewise, the pulse width of chirped pulses is determined from the Fourier transform of the spectrum accounting for a spectral phase corresponding to the excess GDD. The latter is determined from the known amount of excess fused silica in the beams. The pulse widths obtained by this procedure are in good agreement with the results of the autocorrelation measurements. Independent second-harmonic frequency-resolved optical-gating (FROG) measurements[12] confirm the results of this pulse characterization procedure. In particular, the FROG measurements show that the pulses are linearly chirped.

The experiments were carried out with downchirped or upchirped pulses with equal pulse widths of 40 fs, or with 20-fs unchirped pulses, if not mentioned otherwise. The chirp corresponds to a GDD of ± 300 fs^2. As usual, downchirp refers to the high-energy components being in the leading edge of the pulse ($d\omega/dt < 0$). We examined different chirp configurations: (i) pump pulse chirped and probe pulse unchirped (pump-chirp DT), (ii) probe pulse chirped and pump pulse unchirped (probe-chirp DT), and (iii) pump and probe pulses chirped (equal-chirp DT).

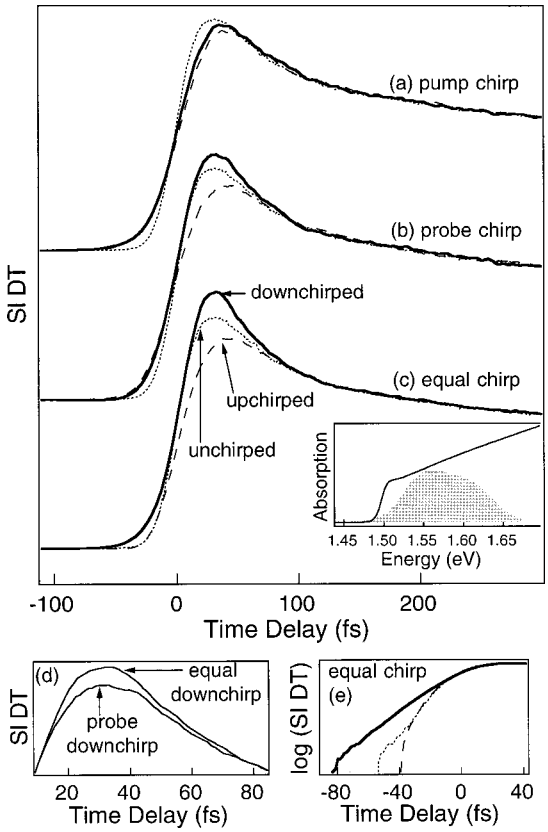

Fig. 1. Spectrally integrated differential transmission (SI DT) for (a) pump chirp, (b) probe chirp, and (c) equal chirp. In (d) the SI DT maxima for equal-downchirp and probe-downchirp are compared. In the logarithmic plot (e) the equal-chirp SI DT data have been normalized. Solid curves: downchirp. Dashed curves: upchirp. Dotted curves: no chirp. Excitation density is $\sim 2 \times 10^{17}\,\text{cm}^{-3}$; $T = 300$ K. Inset in the upper plot: absorption spectrum at room temperature (solid curve) and the excitation spectrum.

We studied a 200-nm-thick $Al_{0.06}Ga_{0.94}As$ bulk semiconductor sample whose GaAs substrate was removed by chemical wet etching to allow for transmission experiments. The sample was glued onto a sapphire substrate, and a broadband antireflection coating was deposited on its air interface. The pulse spectrum spans from the band edge to states high up in the band (see inset of Fig. 1). The excitation carrier density is $N_{\text{exc}} \approx 2 \times 10^{17}\,\text{cm}^{-3}$. All experiments were performed at room temperature.

3. EXPERIMENTAL RESULTS

A. Spectrally Integrated Differential Transmission

Figures 1(a)–1(c) show the SI DT for the different chirp configurations. The zero of the time-delay axis is arbitrarily defined at the 50% point of the SI DT rising edge. For unchirped pulses the maximum pump-induced trans-

mission change ΔT is $\sim 6 \times 10^{-3}$. Around this SI DT maximum, the DT measured with chirped pulses substantially differs from the one measured with unchirped pulses. The chirp influence on the maximum of the SI DT is largest for equal chirp, smaller for probe chirp, and negligible for pump chirp. In all upchirp configurations the maximum is reduced compared with the data for unchirped pulses. For downchirp the influence of pump chirp on the SI DT maximum is small, whereas for the other two downchirp configurations the SI DT maximum is clearly enhanced. The overall highest maximum is achieved for equal downchirp; see Fig. 1(d). The differences vanish after a few tens of femtoseconds, leading to an ultrafast, sub-100-fs time window in which the SI DT is increased.

Moreover, the chirp has an unexpected influence on the rising edge of the SI DT. Figure 1(e) shows that, for the equal-chirp configuration, the rising edge does not reflect the pulse width. The curves for unchirped pulses and equal-upchirped pulses show a similar rise, even though the pulse widths are different by a factor of 2. For equal-downchirped and equal-upchirped pulses the rises are different, although the pulse widths are equal.

Figure 2 shows that the chirp influence in the equal-chirp configuration scales monotonically with the magnitude of the chirp. A GDD range from -300 fs^2 to $+600$ fs^2 is shown in Fig. 2. A negative sign of the GDD corresponds to downchirp. With increasing upchirp the SI DT maximum is reduced. Note also that the SI DT at negative time delays can become negative for upchirp. For downchirp the maximum is increased. This increase saturates at approximately -400 fs^2.

In order to verify that the chirp effects are related to the continuum nonlinearity, we carried out measurements on a pure GaAs sample, where the probe and the pump spectra do not overlap with the band edge. It is observed that the chirp has the same effect in both the GaAs and the AlGaAs samples. This shows that the chirp effects are indeed due to the continuum and not to the excitonic nonlinearity.

We also performed measurements in which other experimental parameters were varied: (i) The center energies of the excitation and probe spectra were varied within the continuum of the AlGaAs sample. (ii) Experiments with shorter 15-fs pulses were carried out. These pulses were broadened to 60 fs by chirping. (iii) The excitation carrier density was varied from $N_{\mathrm{exc}} \approx 5 \times 10^{16}\,\mathrm{cm}^{-3}$ to $N_{\mathrm{exc}} \approx 5 \times 10^{17}\,\mathrm{cm}^{-3}$. (iv) We changed the pump–probe configuration from linear perpendicular polarizations to linear parallel polarizations. In all four cases, similar chirp effects are observed. This shows that the chirp effects are of a general nature and are not the result of a unique experimental situation.

With respect to applications we note that the equal-chirp configuration, which gives the strongest enhancement of the SI DT maximum, is particularly interesting for semiconductor saturable absorber applications in laser physics. In ultrafast pulse generation the pulse can be shaped or stabilized by the transmission changes the pulse itself induces in a saturable absorber in the laser cavity. This situation comes closest to a pump–probe measurement when the pump and the probe pulses have identical spectra and chirps. Chirp of the right sign can optimize the absorber modulation in an ultrafast time window and facilitate pulse formation. The single-chirp (pump-chirp or probe-chirp) configurations are of interest for schemes involving several pulses with different chirps. Our results show that chirping of the probe pulse leads to larger effects than chirping of the pump pulse. In the language of switching this means that chirping of the signal pulse gives a larger effect than chirping of the gating pulse.

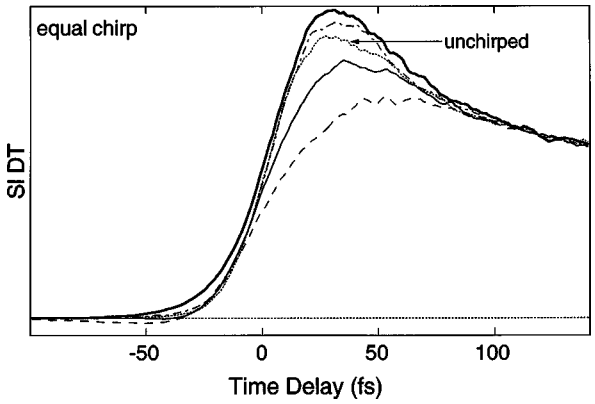

Fig. 2. Equal-chirp configuration: spectrally integrated differential transmission for different magnitudes of the chirp. Excess GDD is -300 fs^2 (highest maximum), -150 fs^2, 0 fs^2, $+300$ fs^2, and $+600$ fs^2 (lowest maximum).

B. Spectrally Resolved Differential Transmission: Unchirped Pulses

Spectrally resolved DT measurements were performed to obtain physical insight into the mechanisms that lead to the chirp effects seen in the SI DT experiments. To pinpoint the chirp-dependent effects in the SR DT, we recall the properties of the SR DT for unchirped pulses that have been studied earlier.[13–20] We refer here to SR DT as the product of the pump-induced transmission change times the probe intensity $\Delta T I_{\mathrm{probe}}$ because we want to link the SR DT data as closely as possible to the SI DT data. With this definition the SI DT is directly given by the area under the SR DT curve.

Figure 3 shows the SR DT for unchirped pump and probe pulses at a negative time delay corresponding to the onset of the rise of the SI DT and at a time delay close to zero. At the band edge, at $\sim$1.49 eV, contributions of bandgap renormalization[21] and excitonic line broadening[13] can be seen. The DT contributions that are essential for the chirp effects result from the continuum nonlinearity, as discussed above. In the continuum the spectral hole (bleaching, $\Delta T I_{\mathrm{probe}} > 0$) builds up from a transient oscillation.[14] At early times the bleaching is already strongly redshifted with respect to the pump spectrum. At high photon energies, reduced transmission ($\Delta T I_{\mathrm{probe}} < 0$) is observed. The initial redshift of the spectral hole and the negative DT at high energies have been explained in terms of dynamic Fermi edge-singularity effects.[15] Moreover, coherent local-field effects can also lead to these signatures in the DT spectrum.[20] While the negative DT vanishes at later

times, the bleaching builds up and shifts toward the band edge a s the carrier distribution thermalizes.[13,16]

C. Spectrally Resolved Differential Transmission: Equally Chirped Pulses

The asymmetric shape of the spectral hole and its dynamics during the early stages of thermalization observed for unchirped pulses build the foundation for the observed strong chirp effects for equal chirp. For chirped pulses, different spectral regions are excited and probed with different efficiency depending on the time delay and the chirp of the pulses. The SI DT maximum is increased if the readout of positive contributions is maximized. This concept will be explained in more detail in the following.

Figure 4 shows DT spectra for equal downchirp and equal upchirp at a small negative time delay approximately corresponding to the onset of the rise of the SI DT. The ratio between positive and negative DT contributions varies significantly depending on the sign of the chirp and compared with zero chirp (compare Figs. 3 and 4). For equal downchirp, only bleaching is observed, while strongly enhanced negative DT is obtained for equal upchirp. To explain these observations, we recall that efficient probing of the transmission change induced by a pump-energy component is possible only with time-delayed or simultaneously arriving probe components. This approach considers only the direct probe-transmission term. We will comment on the grating coupling term[22] later. The perturbed free-induction decay term is negligible for excitation of an inhomogeneously broadened continuum.[23]

The insets in Fig. 4 schematically show the pump- and probe-energy components as a function of time for both chirp configurations. In the upper inset, τ_0 denotes the time delay between pump and probe taken at the center energy E_0 of the pulse spectrum:

$$\tau_0 = t_{\mathrm{probe}}(E_0) - t_{\mathrm{pump}}(E_0). \quad (1)$$

The inset shows the case $\tau_0 < 0$. Transmission changes induced by the marked pump-energy component can be probed only by the marked time-delayed probe components. Therefore for equal downchirp, probing occurs on the low-energy side of a pump-energy component. Here,

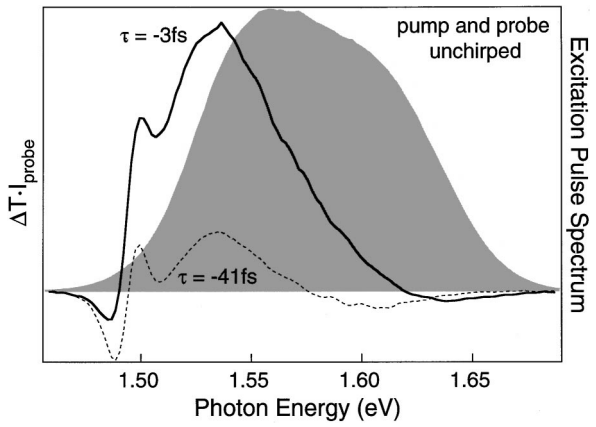

Fig. 3. Differential-transmission spectra $\Delta T I_{\mathrm{probe}}$ for unchirped pump and probe pulses at two pump–probe time delays τ. Shaded area: excitation-pulse spectrum.

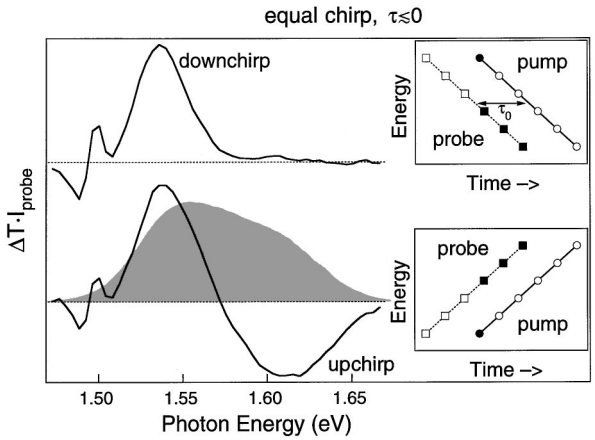

Fig. 4. Differential-transmission spectra at small negative time delay τ for equal downchirp and equal upchirp. Shaded area: excitation-pulse spectrum. Insets: schematic pictures of the pulse energy components versus time for equal downchirp and equal upchirp.

only bleaching can be probed owing to the initial redshift of the spectral hole. In fact, only bleaching is observed for downchirp in Fig. 4. For equal upchirp this situation is reversed. Probing occurs on the high-energy side of a pump-energy component in which the DT is negative. One expects that the negative DT contribution is enhanced in the SR DT, in agreement with the experimental data. Moreover, probing of bleaching at early times for equal downchirp results in an early SI DT rise, while for equal upchirp the efficient probing of negative DT leads to a delayed rise of the SI DT, in agreement with the experimental results of Fig. 1(e).

Summarizing this discussion, the chirp results in a spectral time delay τ_{sp}, given by

$$\tau_{\mathrm{sp}}(E_{\mathrm{probe}}, E_{\mathrm{pump}}) = t_{\mathrm{probe}}(E_{\mathrm{probe}}) - t_{\mathrm{pump}}(E_{\mathrm{pump}}), \quad (2)$$

which depends on the energy separation between the probe- and pump-energy components E_{probe} and E_{pump}. This time delay determines the efficiency with which probe-energy component E_{probe} can read out the transmission changes induced by pump-energy component E_{pump}. This concept is applied to all chirp configurations.

The energy dependence of the readout efficiency also explains the DT data at later times. Figure 5 shows the DT spectra for equal downchirp and equal upchirp for a small positive time delay near the maximum of the SI DT. As the insets illustrate, for upchirp the probing at high energies is still most efficient. In contrast, for downchirp, probing at low energies is most efficient. We recall that the SR DT is intrinsically asymmetric since the bleaching is shifted to lower energies with respect to the exciting-pulse spectrum. This has been shown for unchirped pulses in Fig. 3. Therefore efficient probing at low energies results in a larger positive DT signal than does efficient probing at high energies, as observed in Fig. 5. In the SI DT this manifests itself in the higher maximum for equal downchirp. In essence the chirp of the probe pulse has to be matched to the shape and the dynamics of the positive DT contributions in order to increase the SI DT maximum.

The chirp dependence of the SR DT in the equal-chirp configuration was analyzed at two time delays in Figs. 4 and 5. To investigate the time evolution, we analyzed the SR DT in the complete energy–time plane, as shown in the $\Delta T I_{\mathrm{probe}}$-contour plots in Fig. 6. At early time delays, for equal downchirp, only bleaching is probed, while strongly enhanced negative DT can be seen for equal upchirp, in agreement with Fig. 4. This explains the rise dynamics of the SI DT in Fig. 1(e). For equal downchirp the SI DT rising edge smears out owing to the probing of bleaching at early time delays. For equal upchirp, positive and negative DT contributions are probed simultaneously during the early stages of pulse overlap, and therefore the buildup of a positive SI DT signal is prevented. Even a negative SI DT signal can result at these time delays for equal upchirp. The different shape of the DT spectra near the SI DT maximum, shown in Fig. 5, can also be seen in Fig. 6.

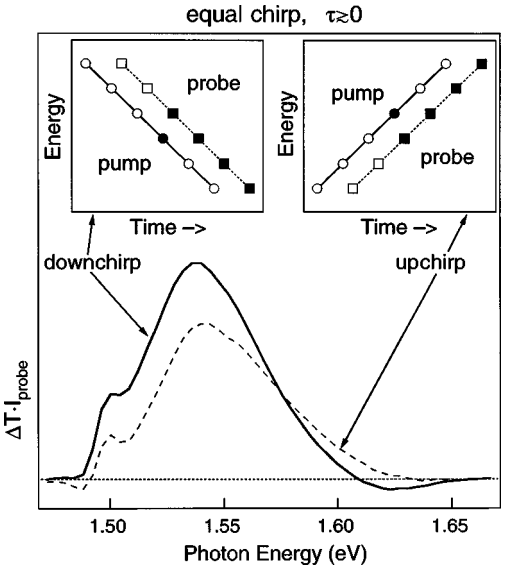

Fig. 5. Differential-transmission spectra at small positive time delay τ for equal downchirp and equal upchirp. Insets: schematic pictures of the pulse energy components versus time for equal downchirp and equal upchirp.

The chirp influence is extracted in Fig. 7. For this purpose the difference of the $\Delta T I_{\mathrm{probe}}$-contour plots, equal downchirp minus equal upchirp, is plotted. This procedure eliminates the chirp-independent contributions to the DT signal and emphasizes the chirp effects. A zero-difference signal corresponds to negligible chirp influence. We like to follow the chirp influence along the SI DT curve and to compare chirp effects for different chirp configurations at the onset of the SI DT curve, the 50% point, and close to the maximum. Therefore we use the same definition of delay zero as before, where zero is assumed to be at the 50% point of the SI DT rising edge.

With respect to the interpretation of the difference contour plot for equal chirp we note that all differences can be understood from the results shown in Figs. 4–6. For

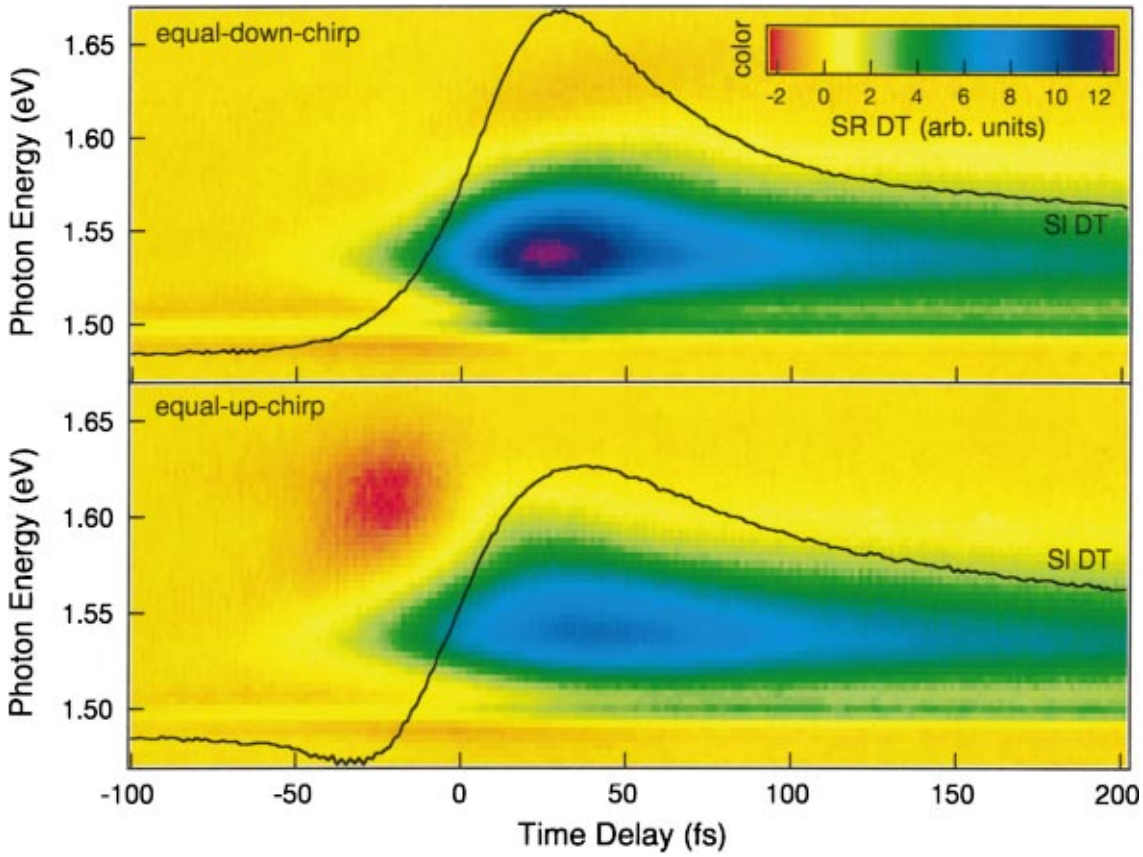

Fig. 6. Contour plots of the differential transmission $\Delta T I_{\mathrm{probe}}$ in the plane of time delay and photon energy for equal downchirp and equal upchirp. Solid curves: spectrally integrated differential transmission.

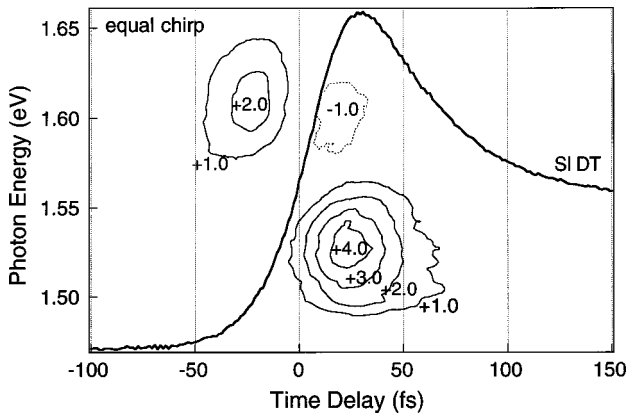

Fig. 7. Equal-chirp configuration: differences of the differential transmission ΔTI_{probe}-contour plots in Fig. 6 (downchirp minus upchirp) in the plane of time delay and photon energy. Shown are contour lines representing equal heights in arbitrary units. Solid curves: positive differences. Dashed curves: negative differences. Thick curve: spectrally integrated differential transmission for equal downchirp.

example, the chirp effects explained in Fig. 5 give rise to the positive and negative contributions at the maximum of the SI DT in Fig. 7. We recall that probing at low energies is more efficient for downchirp than for upchirp. This leads to the positive differences at low energies. In the same way the negative contribution at high energies can be explained. The difference contour plot clearly shows that these differences persist for ~50 fs. At larger time delays the chirp influence is negligible, corresponding to differences of zero. The difference contour plot directly demonstrates the enhancement of the SI DT in an ultrafast time window for equal downchirp, in agreement with Fig. 1. For the following discussion it is important to note that the largest differences in Fig. 7, i.e., the strongest chirp effects for the equal-chirp configuration, are found at time delays close to the maximum of the SI DT.

D. Spectrally Resolved Differential Transmission: Single-Chirp Configurations

In this subsection the SR DT signals are discussed for the pump-chirp and the probe-chirp configurations, i.e., for the configurations in which only the exciting or the readout pulse is chirped. The chirp effects are again explained by qualitative arguments based on different pump- and probe-energy components and their relative time delays. In this simple model it can be understood that the chirp influence on the SI DT maximum in the single-chirp configurations is weaker than for equal chirp. Moreover, the simple qualitative model explains the differences between the two single-chirp configurations.

We first consider the pump-chirp configuration. Figure 8 shows the SR DT for pump upchirp and pump downchirp at the beginning of the rise of the SI DT curve. As one would expect, for early times, bleaching is observed in the spectral region that is excited first. Therefore for pump upchirp, bleaching is observed at low energies, while bleaching is found at high energies for pump downchirp. The pump-downchirp minus pump-upchirp difference contour plot in Fig. 9(a) also reflects this observation. Here, the chirp effects at early time delays correspond to the DT differences with positive (high energies) and negative (low energies) sign.

To explain the differences at later times, we consider a fixed high energy in the contour plot in Fig. 9(a). As one moves along the time axis, the sign of the difference changes. At early times this range is excited for pump downchirp, while it is not for pump upchirp, leading to a positive-downchirp minus upchirp DT difference, as explained above. At a later time this range is excited for pump upchirp, while for pump downchirp the relaxation after the excitation has already decreased the DT signal. This leads to the negative difference at later times. At low energies the situation is reversed.

We now comment on the chirp influence on the SI DT maximum for pump chirp. In this respect the form of the spectral time delay, defined in Eq. (2), is very important. We note that, for the equal-chirp configuration, all pump and probe components at the same energy have the same spectral delay $\tau_{\text{sp}}(E_{\text{probe}} = E_{\text{pump}} = E) = \tau_0 \neq f(E)$. This is not the case for the pump-chirp configuration, as seen from the comparison between the schematic pictures in Figs. 5 and 9. This has substantial impact on the chirp effects observed at the SI DT maximum.

To obtain the SI DT maximum for the pump-chirp configuration, all pump components have to excite the sample because all pump components contribute positive DT to the integrated signal. Therefore if pump and probe components of the same energy are considered, for some energies E, large spectral delays arise at the maximum of the SI DT. This is because $\tau_{\text{sp}}(E_{\text{probe}} = E_{\text{pump}} = E) = f(E)$ is a function of E for pump chirp, as is schematically shown in Fig. 9(a). As a consequence, the chirp effects are already partially smeared out owing to thermalization when the SI DT maximum is reached. This smearing effect can directly be seen in the difference contour plot. Figure 9(a) shows that, for pump chirp, the largest chirp effects occur around the 20% point in the rise of the SI DT. In contrast, for the equal-chirp configuration the largest chirp effects are found close to the maximum of the SI DT since smearing effects are absent; see Fig. 7. For pump chirp the chirp effects at the SI DT maximum are considerably smaller than for equal chirp as a result of the smearing. This smearing effect is the reason for the distinctly different chirp influence seen in the SI DT for equal chirp and pump chirp in Fig. 1.

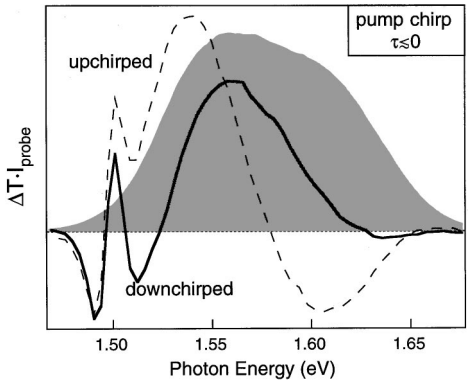

Fig. 8. Differential-transmission spectra at small negative time delay τ for pump downchirp and pump upchirp. Shaded area: excitation-pulse spectrum.

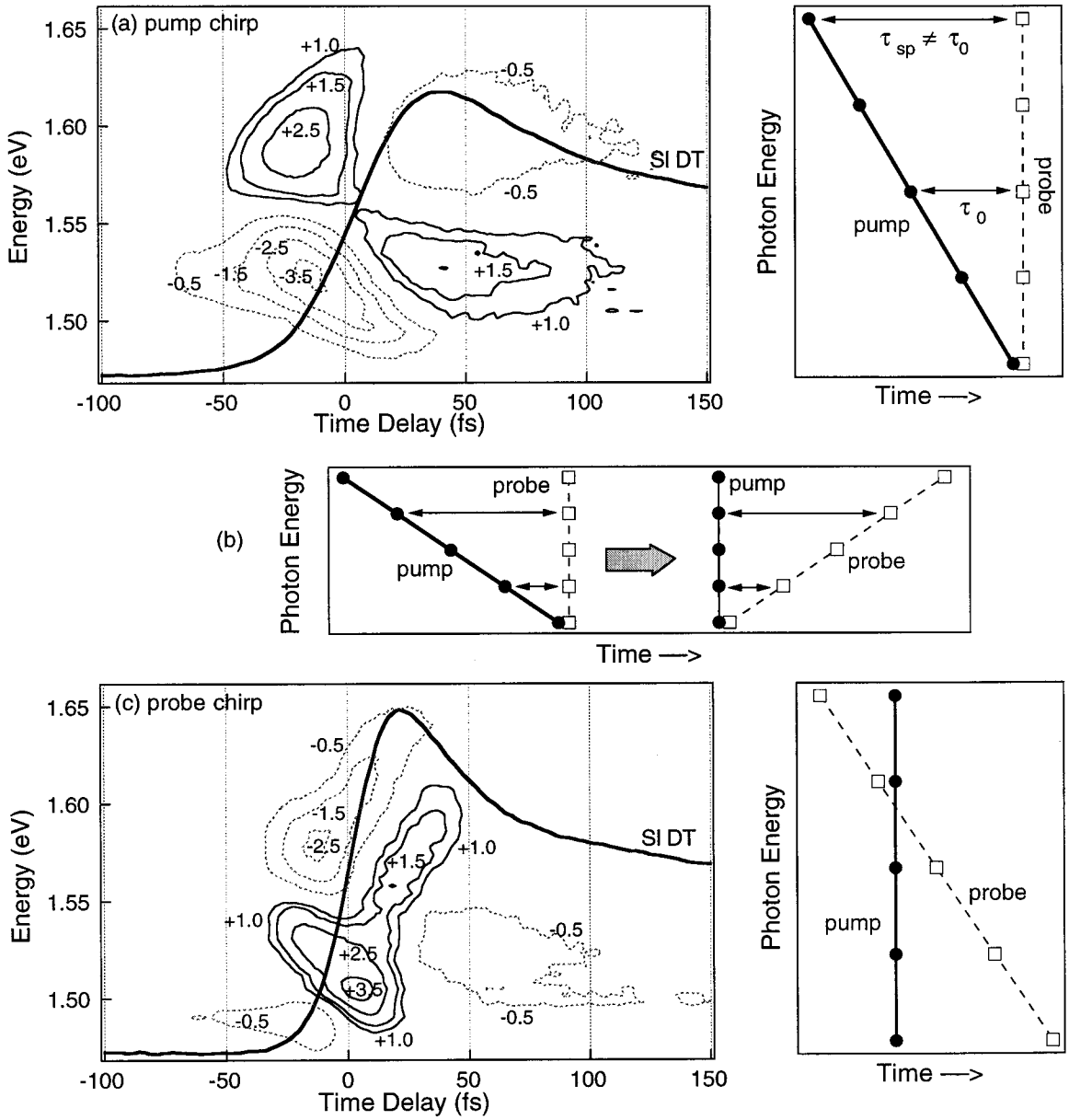

Fig. 9. Differences of the differential transmission ΔTI_{probe} contours (downchirp minus upchirp) in the plane of time delay and photon energy for (a) pump chirp and (c) probe chirp. Shown are contour curves representing equal heights in arbitrary units. Solid curves: positive differences. Dashed curves: negative differences. In (a) and (c) the same arbitrary units are used as in Fig. 7. Thick curves: spectrally integrated differential transmission for downchirp. The schematic pictures show the pump and probe pulse energy components versus time for (a) pump downchirp, (b) pump downchirp and probe upchirp, and (c) probe downchirp.

We now discuss the probe-chirp configuration. The chirp effects in the SR DT can be understood by comparison with the pump-chirp configuration. When switching, for example, from pump downchirp to probe upchirp, the spectral delay between all pump and probe components at the same energy $\tau_{\text{sp}}(E_{\text{probe}} = E_{\text{pump}} = E)$ does not change. This is shown in Fig. 9(b). As the spectral delay determines the probing efficiency of DT contributions, pump downchirp and probe upchirp are in this sense symmetric configurations: pump downchirp $\triangleq$ probe upchirp. The same is true for pump upchirp and probe downchirp. Therefore one would expect qualitatively similar structures in the downchirp minus upchirp difference contours for pump and probe chirp. Only the sign of these structures should change between pump chirp and probe chirp. Indeed, this is observed in Figs. 9(a) and 9(c).

While the chirp effects in the SR DT for pump and probe chirp are qualitatively similar, the chirp effects in the SI DT are quantitatively different, as shown in Figs. 1(a) and 1(b). In particular, probe downchirp increases the SI DT maximum as compared with the unchirped configuration, whereas pump chirp does not. Therefore the simple argument dealing with the symmetry in the spectral delay alone cannot explain the chirp dependence of the SI DT. In fact, for probe downchirp, the smearing effect is reduced. For pump chirp, all probe energy components have to follow the pump in order to reach the SI DT

maximum because all pump-energy components contribute to the bleaching signal. This is shown in the schematic picture in Fig. 9(a) for the example of pump downchirp. In contrast, for probe downchirp, only the low-energy probe components have to follow the pump to obtain the SI DT maximum [see schematic picture in Fig. 9(c)]. This is because the SR DT is intrinsically asymmetric and the highest probe energies would only detect a small-bleaching signal or even negative DT. Therefore the SI DT maximum occurs at smaller spectral delays for probe downchirp than for pump chirp, and the smearing effect is less pronounced. Since the smearing is reduced for probe downchirp, the SI DT maximum can still be manipulated by the chirping. The downchirp of the probe is well matched to the shape and the dynamics of the positive DT contributions and therefore increases the SI DT maximum. In essence, the same arguments apply as for the equal-downchirp configuration.

The difference contour plot for probe chirp in Fig. 9(c) shows the largest positive differences around the 70% point in the rise of the SI DT curve, closer to the SI DT maximum than for the pump-chirp configuration. Large positive differences persist at the SI DT maximum. The large positive differences close to the SI DT maximum result from the probe-downchirp DT signal and are a manifestation of the reduced smearing in this configuration.

In summary of the discussion of the single-chirp configurations, the smearing of the chirp effects owing to large spectral delays at the maximum of the SI DT is very strong for pump chirp. Therefore negligible chirp influence on the maximum of the SI DT is observed for pump chirp. In contrast, for probe downchirp, the SI DT maximum can be manipulated to a certain extent because the smearing effect is reduced. In the equal-chirp configuration this smearing effect is not present at all. All pump and probe components at the same energy have the same time delay. Therefore the influence of chirp on the SI DT maximum is strongest in the equal-chirp configuration.

4. MODELING

In the preceding section we explained all chirp effects by qualitative arguments. Here, we present a quantitative model that confirms the validity of our basic considerations. In essence, the model considers that the spectral time delay determines the efficiency with which a probe-energy component can detect the SR DT induced by a pump-energy component.

The model simplifies the real DT dynamics in some respects. First, our approach mainly considers the direct probe-transmission term and accounts for DT contributions owing to the grating-coupling term[22] only at large negative time delays. For the modeling of the chirp influence on the SI DT maximum, this simplification is justified by the following experimental result. We performed DT measurements when pump and probe had linear parallel polarizations instead of linear perpendicular polarizations. In both configurations we observe the same chirp effects on the SI DT maximum. As the grating-coupling term is weaker for linear-perpendicular than for linear-parallel polarizations,[24] we can conclude that the direct probe-transmission term, and not the grating-coupling term, dominates the chirp effects on the SI DT maximum. Second, it is assumed in the model that the DT contributions of different pump-energy components add up linearly. Therefore the model is not valid in the regime of strongly saturated absorption. Moreover, we consider only continuum nonlinearities and no excitonic effects. With the focus on the chirp effects this is justified, as shown in the previous sections.

With respect to the continuum nonlinearity we consider the shape and the dynamics of the DT response for continuum excitation in a qualitative way. To this end, we define a DT model function, as explained in detail in the following. This model function includes phase-space filling[1] and many-body Coulomb effects[1] as well as the thermalization of the optically excited carriers on short time scales.[19,25] For the construction of the model function, we have taken advantage of the results of previous DT spectroscopy work for semiconductor continuum excitation.[13–20] The model function qualitatively describes the complex DT dynamics in a semiconductor and allows for the simulation of the main trends seen in the chirp-control experiments. However, quantitative agreement between experimental and calculated results cannot be expected since this is beyond the scope of our approach.

We assume pump and probe pulses with Gaussian spectra with a spectral FWHM of 90 meV, centered 90 meV above the band edge. This leads to a bandwidth-limited pulse duration of $T_{\mathrm{pulse}} = 20$ fs. For the chirped pulses a GDD of ± 330 fs^2 is assumed, similar to the GDD in the experimental part.

As a first step, we decompose the broadband pump spectrum into 20-meV broad pump-energy components. We define the shape of the transmission changes induced by a single pump-energy component at different time delays τ, as shown by the DT model function in Fig. 10. At $\tau = -T_{\mathrm{pulse}}$, a ΔT spectrum with the shape of a transient oscillation[14] is assumed. This spectrum evolves linearly with time into the ΔT spectrum at $\tau = 0$. For this DT spectrum we assume a bleaching signal that is redshifted with respect to the exciting pump-energy component and negative DT at the high-energy side of the pump component,[15,20] as shown in Fig. 10. This spectrum evolves linearly with time into the ΔT spectrum at $\tau = +T_{\mathrm{pulse}}$. At $\tau = +T_{\mathrm{pulse}}$ the ΔT spectrum extends

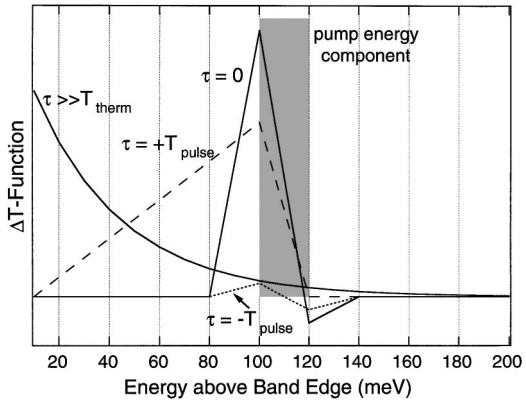

Fig. 10. Model function for the transmission changes ΔT induced by the shaded pump-energy component versus the excess energy above the band edge at four different time delays τ.

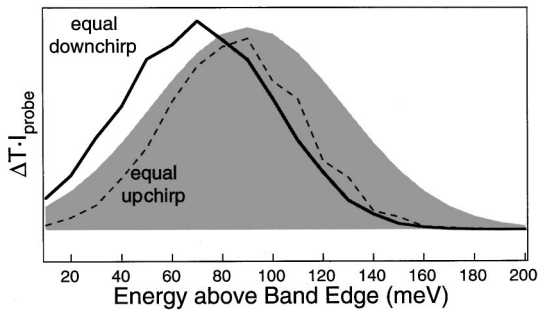

Fig. 11. Calculated differential-transmission spectra for equal downchirp and equal upchirp at a delay corresponding to the rising edge of the SI DT. Shaded area: excitation-pulse spectrum assumed for the calculation.

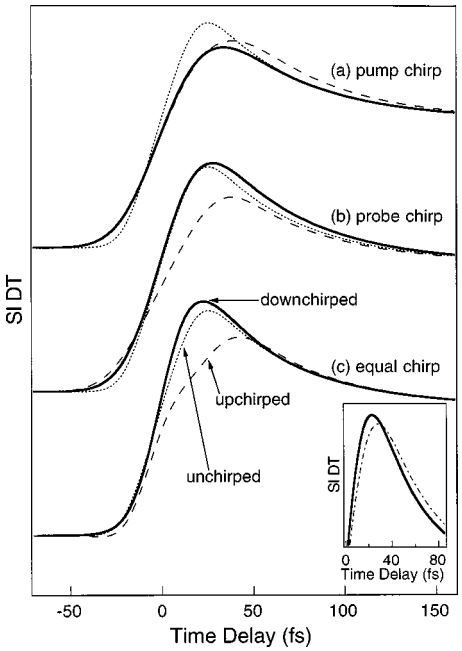

Fig. 12. Calculated spectrally integrated differential transmission (SI DT) for (a) pump chirp, (b) probe chirp, and (c) equal chirp. Solid curves: downchirp. Dashed curves: upchirp. Dotted curves: no chirp. The inset compares the calculated SI DT maxima for equal downchirp (solid curve) and probe downchirp (dashed–dotted line).

down to the band edge[19] and the negative DT disappears;[15] see Fig. 10. For later times the ΔT spectrum exponentially approaches a thermalized distribution[16] with the thermalization time constant $T_{\text{therm}} = 50\,\text{fs}$. The thermalized distribution is approximated by a Boltzmann function with a thermal energy of 35 meV. The integral of the ΔT spectra increases linearly from $\tau = -T_{\text{pulse}}$ to $\tau = +T_{\text{pulse}}$ and remains constant at later times. It is directly proportional to the intensity of the pump-energy component. The main features of the DT model function were verified by additional experiments with a broadband probe and a spectrally filtered pump with a FWHM of ~20 meV.

The calculation proceeds as follows. For a given time delay τ_0, the spectral delay τ_{sp} between a fixed pump component E_{pump} and a fixed probe component E_{probe} is calculated according to the chirp in the pump and the probe pulse. We then convolute the model function $M(E_{\text{pump}}, E_{\text{probe}}, \tau_{\text{sp}})$ for the fixed pump and probe components E_{pump} and E_{probe} with the probe pulse, which is assumed to have a Gaussian temporal profile:

$$\Delta T(E_{\text{pump}}, E_{\text{probe}}, \tau_{\text{sp}}) = \int_{-\infty}^{\infty} M(E_{\text{pump}}, E_{\text{probe}}, t') \times \exp\left[-\frac{4 \ln 2 (\tau_{\text{sp}} - t')^2}{T_{\text{pulse}}^2}\right] dt'. \tag{3}$$

We then calculate the transmission change induced by the fixed pump-energy component at all probe energies and sum over all pump-energy components. Finally, we multiply this ΔT spectrum with the probe spectrum. As an example, the resulting $\Delta T I_{\text{probe}}$ spectra are shown in Fig. 11 for equal downchirp and equal upchirp at a delay corresponding to the rising edge of the SI DT. The comparison of the calculated SR DT in Fig. 11 and the measured one in Fig. 5 shows that the main chirp effect is reproduced. The SR DT for equal downchirp shows enhanced DT at low energies owing to the more effective probing in this range.

Integration of the $\Delta T I_{\text{probe}}$ spectra yields the SI DT signal. Varying the time delay τ_0 allows for the construction of the whole SI DT curve. Calculated curves are shown in Fig. 12 for all possible chirp configurations. The calculation reproduces the main chirp effects, in good qualitative agreement with the experimental results in Fig. 1. In particular, the equal-downchirp configuration yields the overall highest SI DT maximum in the calculation. For probe downchirp the SI DT maximum is also increased, while all other chirp configurations result in a reduced SI DT maximum compared with the unchirped SI DT. The difference at the maximum between downchirp and upchirp is smallest for the pump-chirp configuration, in agreement with the experimental data.[26]

In summary, the simple model reproduces the main chirp effects observed in the experiments. Since the model is based on the direct probe-transmission term, this proves that this term is mainly responsible for the chirp effects in the SI DT signal for broadband excitation of the semiconductor continuum. We like to stress that the model is quite general. With this model, chirp effects owing to the direct probe-transmission term can also be estimated for other systems if the model function is changed appropriately.

5. CONCLUSIONS

We have presented a comprehensive experimental study and a simple quantitative model of chirp effects in differential-transmission experiments for broadband excitation of the semiconductor continuum. Our results show that chirping of 20-fs pulses allows one to manipulate the broadband-continuum nonlinearity despite the ultrafast intraband relaxation in the semiconductor continuum. Our data demonstrates that the maximum of the spectrally integrated differential transmission can be manipulated in a switching window of only a few tens of femtoseconds. The largest enhancement of this maximum is achieved when both the pump and the probe

pulses are downchirped. If only one of the pulses is chirped, an increase of the SI DT maximum is obtained only for probe downchirp.

Spectrally resolved studies explain these results. Chirp control of the broadband-continuum nonlinearity in a semiconductor is possible for the following reason: the differential transmission induced by a certain pump-energy component is asymmetric with respect to the pump spectrum and changes its magnitude and spectral position with time. Therefore appropriate chirping allows for the optimization of the readout of the differential-transmission signal. The quantitative model of Section 4 confirms this picture.

We expect that the mechanism for chirp control exploited in our study may also be effective in other systems with densely spaced optical excitations, which strongly interact. Our results should have impact on ultrafast switching applications as well as on fundamental studies of ultrafast nonlinearities.

ACKNOWLEDGMENTS

We acknowledge experimental help from L. Gallmann. This work has been supported by the Swiss National Science Foundation.

*E-mail address: kunde@iqe.phys.ethz.ch.

REFERENCES AND NOTES

1. J. Shah, *Ultrafast Spectroscopy of Semiconductors and Semiconductor Nanostructures* (Springer-Verlag, Berlin, 1996).
2. R. Takahashi, Y. Kawamura, and H. Iwamura, "Ultrafast 1.55 μm all-optical switching using low-temperature-grown multiple quantum wells," Appl. Phys. Lett. **68**, 153–155 (1996).
3. H. S. Loka and P. W. E. Smith, "Ultrafast all-optical switching in an asymmetric Fabry–Pérot device using low-temperature-grown GaAs," IEEE Photonics Technol. Lett. **10**, 1733–1735 (1998).
4. S. Gupta, J. F. Whitaker, and G. A. Mourou, "Ultrafast carrier dynamics in III–V semiconductors grown by molecular-beam epitaxy at very low substrate temperatures," IEEE J. Quantum Electron. **28**, 2464–2472 (1992).
5. D. S. Chemla, D. A. B. Miller, P. W. Smith, A. C. Gossard, and W. Wiegmann, "Room temperature excitonic nonlinear absorption and refraction in GaAs/AlGaAs multiple quantum well structures," IEEE J. Quantum Electron. **QE-20**, 265–275 (1984).
6. A. M. Weiner, "Femtosecond optical pulse shaping and processing," Prog. Quantum Electron. **19**, 161–237 (1995).
7. J. J. Baumberg, B. Huttner, R. A. Taylor, and J. F. Ryan, "Dynamic contributions to the optical Stark effect in semiconductors," Phys. Rev. B **48**, 4695–4706 (1993).
8. J.-P. Foing, M. Joffre, J.-L. Oudar, and D. Hulin, "Coherence effects in pump–probe experiments with chirped pump pulses," J. Opt. Soc. Am. B **10**, 1143–1148 (1993).
9. J. Kunde, U. Siegner, S. Arlt, F. Morier-Genoud, and U. Keller, "Chirp-controlled ultrafast optical nonlinearities in semiconductors," Appl. Phys. Lett. **73**, 3025–3027 (1998).
10. U. Keller, K. J. Weingarten, F. X. Kärtner, D. Kopf, B. Braun, I. D. Jung, R. Fluck, C. Hönninger, N. Matuschek, and J. Aus der Au, "Semiconductor saturable absorber mirrors (SESAM's) for femtosecond to nanosecond pulse generation in solid-state lasers," IEEE J. Sel. Top. Quantum Electron. **2**, 435–453 (1996).
11. N. Matuschek, F. X. Kärtner, and U. Keller, "Analytical design of double-chirped mirrors with custom-tailored dispersion characteristics," IEEE J. Quantum Electron. **35**, 129–137 (1999).
12. K. W. DeLong, R. Trebino, J. Hunter, and W. E. White, "Frequency-resolved optical gating with the use of second-harmonic generation," J. Opt. Soc. Am. B **11**, 2206–2215 (1994).
13. W. H. Knox, C. Hirlimann, D. A. B. Miller, J. Shah, D. S. Chemla, and C. V. Shank, "Femtosecond excitation of nonthermal carrier populations in GaAs quantum wells," Phys. Rev. Lett. **56**, 1191–1193 (1986).
14. B. Fluegel, N. Peyghambarian, G. Olbright, M. Lindberg, S. W. Koch, M. Joffre, D. Hulin, A. Migus, and A. Antonetti, "Femtosecond studies of coherent transients in semiconductors," Phys. Rev. Lett. **59**, 2588–2591 (1987).
15. J.-P. Foing, D. Hulin, M. Joffre, M. K. Jackson, J.-L. Oudar, C. Tanguy, and M. Combescot, "Absorption edge singularities in highly excited semiconductors," Phys. Rev. Lett. **68**, 110–113 (1992).
16. S. Hunsche, H. Heesel, A. Ewertz, H. Kurz, and J. H. Collet, "Spectral-hole burning and carrier thermalization in GaAs at room temperature," Phys. Rev. B **48**, 17818–17826 (1993).
17. J. H. Collet, S. Hunsche, H. Heesel, and H. Kurz, "Influence of electron-hole correlations on the absorption of GaAs in the presence of nonthermalized carriers," Phys. Rev. B **50**, 10649–10655 (1994).
18. S. Bar-Ad, P. Kner, M. V. Marquezini, D. S. Chemla, and K. El Sayed, "Carrier dynamics in the quantum kinetic regime," Phys. Rev. Lett. **77**, 3177–3180 (1996).
19. F. X. Camescasse, A. Alexandrou, D. Hulin, L. Bányai, D. B. Tran Thoai, and H. Haug, "Ultrafast electron redistribution through Coulomb scattering in undoped GaAs: experiment and theory," Phys. Rev. Lett. **77**, 5429–5432 (1996).
20. K. El Sayed and C. J. Stanton, "Line-shape analysis of differential transmission spectra in the coherent regime," Phys. Rev. B **55**, 9671–9678 (1997).
21. H. Haug and S. Schmitt-Rink, "Basic mechanisms of the optical nonlinearities of semiconductors near the band edge," J. Opt. Soc. Am. B **2**, 1135–1142 (1985).
22. C. H. Brito Cruz, J. P. Gordon, P. C. Becker, R. L. Fork, and C. V. Shank, "Dynamics of spectral hole burning," IEEE J. Quantum Electron. **24**, 261–266 (1988).
23. J. P. Sokoloff, M. Joffre, B. Fluegel, D. Hulin, M. Lindberg, S. W. Koch, A. Migus, A. Antonetti, and N. Peyghambarian, "Transient oscillations in the vicinity of excitons and in the band of semiconductors," Phys. Rev. B **38**, 7615–7621 (1988).
24. Z. Vardeny and J. Tauc, "Picosecond coherence coupling in the pump and probe technique," Opt. Commun. **39**, 396–400 (1981).
25. T. Elsaesser, J. Shah, L. Rota, and P. Lugli, "Initial thermalization of photoexcited carriers in GaAs studied by femtosecond luminescence spectroscopy," Phys. Rev. Lett. **66**, 1757–1760 (1991).
26. The slight deviation between experimental and calculated SI DT curves for pump chirp may be caused by the underestimation of chirp effects owing to the grating-coupling term, previously observed in SR DT measurements.[8] Underestimating grating-coupling-term effects may lead to small but noticeable deviations for pump chirp for which chirp effects owing to the direct-probe transmission term are weakest.